Effect of Cooling Rate on the Precipitation Characteristics of Cast Al–Si–Cu Alloy

M. Okayasu [a, *], N. Sahara [a], M. Touda [b]

[a] Graduate School of Natural Science and Technology, Okayama University
3-1-1 Tsushimanaka, Kita-ku, Okayama city, Okayama, 700-8530, Japan
[b] Kyowa Casting Co., Ltd.
5418-3 Nishi Ebara-cho, Ibara city, Okayama, 715-0006, Japan
* Corresponding author. E-mail address: mitsuhiro.okayasu@utoronto.ca

Abstract

The influence of the cooling rate on the extent of precipitation hardening of cast aluminum alloy (ADC12) was investigated experimentally. This study explored the cooling rate of the solidification of Cu in the α-Al phase to improve the mechanical properties of ADC12 after an aging process (Cu based precipitation hardening). The solid solution of Cu occurred in the α-Al phases during the casting process at cooling rates exceeding 0.03 °C/s. This process was replaced with a solid solution process of T6 treatments. The extent of the solid solution varied depending on the cooling rate; with a higher cooling rate, a more extensive solid solution was formed. For the cast ADC12 alloy made at a high cooling rate, high precipitation hardening occurred after low-temperature heating (at 175 °C for 20 h), which improved the mechanical properties of the cast Al alloys. However, the low-temperature heating at the higher temperature for a longer time decreased the hardness due to over aging.

1. Introduction

Due to the demand for vehicle weight reduction to reduce gas emissions and global warming, age-hardenable aluminum alloys have recently attracted significant attention [1]. There are several aluminum alloys categorized with wrought and cast alloy series. Because casting technologies have technical advantages to produce the components with thin walls and complicated geometries with high productivity, various automotive parts, such as transmission case, engine block, and housing, have been produced. However, Al alloys have not been employed satisfactorily in automobile parts, due to the poor material strength of cast Al alloys. Many automobile parts are still made of iron and steel, although attempts have been made to replace iron-based automotive parts with cast aluminum alloys. Rana et al. have reported that the use of cast Al-

alloys is still limited for structure-critical applications compared with wrought Al alloys, even though casting is a more economical production method [2].

To improve the mechanical properties of cast Al alloys, grain size is controlled by the cooling rate [3, 4, 5]. One of the results is that an increase of solidification cooling rate reduces the secondary dendrite arm spacing (SDAS), which enhances the tensile strength as well as the failure elongation [3]. Another approach for creating high-strength cast Al alloys is by using metastable precipitates via a solid solution process followed by aging (T6 treatment) [6]. The precipitation sequence of Al–Cu alloy (T6) is as follows: supersaturated solid solution → Guinier–Preston (G.P.) I zones→ $\theta'' \rightarrow \theta' \rightarrow$ stable θ (CuAl$_2$, equilibrium) [7]. Several studies have examined this sequence and attempted to correlate the phase decomposition in detail with the structures and composition of the

metastable phases. In this instance, Al–Cu alloy is heated to approximately 500°C for 10 h followed by water quenching to dissolve the Cu in the α-Al matrix. The material is then subjected to low-temperature heating (e.g., at 180°C for 10 h) to precipitate CuAl₂ in the α-Al matrix. However, T6 treatment is not suitable for cast Al alloys, because of the creation of defects by high-temperature heating of solid solution (blister defect) [8].

In our previous study where high-strength cast aluminum alloy was created, it was clarified that the solid solution process could be removed to achieve the precipitation hardening of high-pressure die-casting aluminum alloys, [9]. The solid solution process can be replaced by a rapid solidification process of high-pressure die-casting [10, 11], even though the proper cooling rate of the solidification process has not been clarified. This information is important to make high-strength cast Al alloy via precipitation hardening without a solid solution process of T6 treatments. Thus, this study examines the effect of the solidification rate on the precipitation hardening of cast Al alloy.

2. Experimental procedures

2.1. Material

The cast aluminum alloy used in this study was a commercial Al–Si–Cu alloy (ADC12): Al–10.4Si–1.7Cu–0.3Mg–0.9Fe (mass%). The cast samples were made by gravity casting at different cooling speeds. A 95-g sample of ADC12 was melted at 630°C and was poured into a mold made of hardened steel before solidification at room temperature. The size of the cast samples was designed with 60 mm × 60 mm × 15 mm. For the solidification of the molten ADC12 alloy, the following cooling processes were employed: air cooling in steel (GC) and ceramic molds (GC and AC, respectively), and furnace cooling at low and high temperatures (FAC and FC, respectively) in a ceramic mold. Steel and ceramic molds were used to change the thermal insulation properties. In the FAC process, cool air (25°C) was charged into the furnace, while the furnace cooling was conducted for the FC process by turning off the furnace after melting the ADC alloy in the ceramic mold. Figure 1(a) shows a schematic representation of the cooling processes.
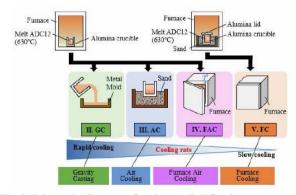

Fig. l. Schematic diagram of various solicUfication processes to obtain different cooling rate

2.2. Precipitation hardening

To examine the extent of precipitation hardening in ADC12 samples, low-temperature aging (LTA) was conducted at 175°C and 220°C for 1–96 h without the ST process. Here, this approach is used to investigate the suitable cooling rate of the casting process to make a solid solution of Cu elements in the α-Al matrix. Note that the heating temperatures of the LTA (175 °C and 220 °C) were determined based on our previous study [12].

2.3. Mechanical testing and microstructural observations

The mechanical properties (hardness and tensile strength) of the cast ADC12 were investigated. The material hardness was examined using a micro-Vickers hardness and a dynamic ultra-micro-hardness nanoindentation system. The surfaces of the test samples were all polished to a mirror level before the hardness test. Diamond indentation loads were applied to the sample surface at 9.8 N and 0.1 mN using the micro-Vickers hardness and the nanoindentation tester, respectively. Different loading values were adopted to examine the material hardness in the large and small areas of the cast samples.

Tensile properties were investigated at room temperature using rectangular test specimens with dimensions of 6.5 mm × 2.5 mm × 1 mm. The specimens were so-designed due to the size limitation of the cast sample. Tensile tests were conducted on at least three specimens using a 50-kN screw-driven universal testing machine. The tensile stress and tensile strain values were monitored by a data acquisition system in conjunction with a computer through a standard load cell and strain gauge. The loading speed for the tensile test was 1 mm/min until failure.
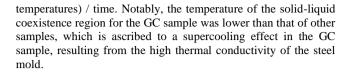
The microstructural characteristics of the cast ADC12 samples subjected to different cooling rates and different heating processes were examined using optical microscopy and electron backscattering diffraction (EBSD) analysis. The EBSD analysis was executed using a scanning electron microscope (SEM) with an accelerating voltage of 15 kN. Furthermore, to examine the precipitation characteristics of the cast ADC12, scanning transmission electron microscopy (STEM) observation was conducted. Before the STEM observation, thin films of ~100 nm were made by mechanical thinning followed by electrolytic polishing with 30% nitric acid and 70% methanol.
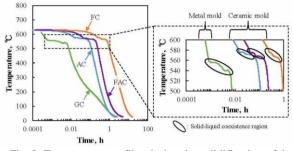
3. Results and discussion

3.1. Microstructural characteristics

Figure 2 shows the temperature profiles during solidification of the cast samples (GC, AC, FAC, and FC), which were directly measured using a thermocouple. The cooling rates were determined as follows from the temperature profiles in the solid-liquid coexistence region [13]: 1.17 °C/s (GC), 0.052 °C/s (AC), 0.030 °C/s (FAC), and 0.006 °C/s (FC), i.e., (liquidus – solidus
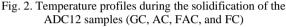
temperatures) / time. Notably, the temperature of the solid-liquid coexistence region for the GC sample was lower than that of other samples, which is ascribed to a supercooling effect in the GC sample, resulting from the high thermal conductivity of the steel mold.

Fig. 2. Temperature profiles during the solidification of the ADC12 samples (GC, AC, FAC, and FC)

Figure 3(a) shows the microstructures of the cast ADC12 samples, representing four different cooling rates (GC, AC, FAC,

and FC samples). Overall, the ADC12 samples consisted of the α-Al phase and eutectic structures with Cu-, Si-, and Fe-based phases. The grain size varied depending on the cooling rate. Table 1 indicates the SDAS values and cooling rates for the four samples of ADC12. The SDAS is correlated with the cooling rate; the higher the cooling rate, the smaller the SDAS. Figure 3(b) shows the microstructures of the above four cast samples after the LTA at 175°C for 3 h, 175°C for 96 h, and 220°C for 96 h. No evident microstructural changes were observed, rather similar eutectic phases were observed after prolonged aging.

Table 1.
Cooling rates and SDAS values for cast ADC12 samples prepared by various processes.

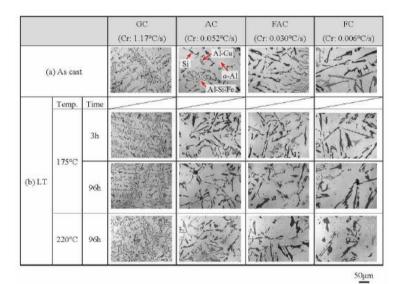|	GC	AC	FAC	FC
Cooling rate (CR), °C/s	1.17	0.052	0.030	0.006
SDAS, μm	13.2	45.0	61.0	95.0

Fig. 3. Micrographs of the cast ADC12 samples obtained using four different cooling rates (i. e., the GC, AC, FAC, and FC samples) and various heating processes

Figure 4 shows the EBSD analysis results for the four cast samples before the LTA. As shown by the inverse pole figure (IPF) maps, the relatively organized crystal orientation of the α-Al matrix is detected for all samples, which could be affected by the unidirectionally solidified ADC12 alloy from the surfaces of the die. Conversely, depending on the sample, different extents of the kernel average misorientation (KAM) were obtained, as indicated by the change in color from dark green to lighter green. The dark green is widely observed in samples with a low cooling rate (FAC and FC), which is ascribed to the low internal strain.
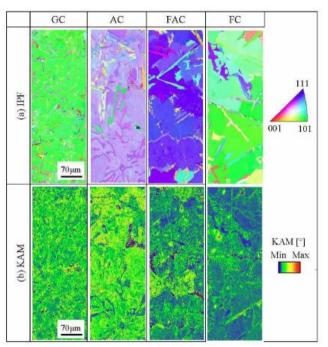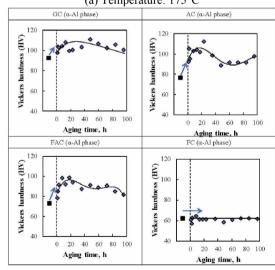
Fig. 4. EBSD analysis (IPF and KAM maps) of the GC, AC, FAC, and FC samples of ADC12 before LT aging.

of GC, AC, and FAC samples increased rapidly upon subjecting them to LTA at 175°C for approximately 20 h, although a slight improvement of hardness is obtained by LTA at 220°C. After aging at 175°C for 20 h, the GC and AC samples displayed high hardness values of 115 HV. The enhancement of the hardness value could be attributed to the different severity of precipitation hardening. In contrast, the hardness values of the three samples decreased when they were over-aged by heating for more than 20 h [12]. Moreover, the hardness profile of the FC sample plateaued and decreased as the heating time increased at 175°C and 220°C, respectively. Note, despite no clear microstructural changes for the cast ADC12 samples after LTA (Figure 3), the hardness values were altered for all samples.

3.2. Mechanical properties

Figure 5 presents the Vickers hardness as a function of aging time at 175°C and 220°C for the four samples. The hardness values
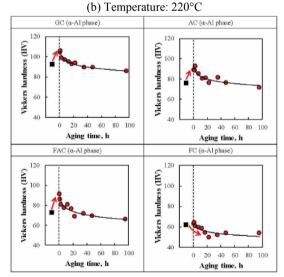

Fig. 5. Vickers hardness as a function of aging time for the GC, AC, FAC, and FC ADC12 samples: (a)175°C and (b) 220°C

To further understand the mechanical properties of the cast ADC12 samples, hardness measurement was conducted only in the α-Al phase using the nanoindentation method. Figure 6(a) presents the hardness values for the four cast samples determined by nanoindentation before and after the LTA (175°C for 3 h). The

hardness values of the GC, AC, and FAC samples increased after the LTA, whereas no clear increase in hardness was observed for the FC sample, following the Vickers hardness test results (Figure 5). Figure 6(b) shows the curves of load (P) against nanoindentation depth (d) for these samples. The elastic constants

of the GC, AC, and FAC samples increased after the LTA, as indicated by an increase in the slopes of their respective P vs. d curves. In contrast, no clear increment in elastic constant was observed for the FC sample. These results are caused by different extents of precipitation in the four samples during the LTA. Figure 7 shows the STEM images of the FAC and FC samples. As seen,

the θ' (CuAl$_2$) metastable phases are observed for the FAC sample leading to precipitation hardening. In contrast, no clear precipitation was observed in the FC sample, where Q (AlMgSiCu) phases are created, explaining its inferior mechanical properties.

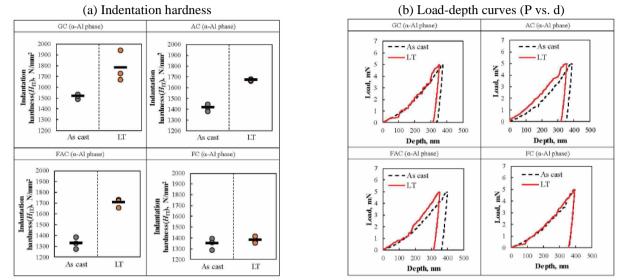(a) Indentation hardness   (b) Load-depth curves (P vs. d)

Fig. 6. (a) Hardness values determined by nano-indentation and (b) curves of load vs. depth before and after the heating processes for the GC, AC, FAC, and FC ADC12 samples
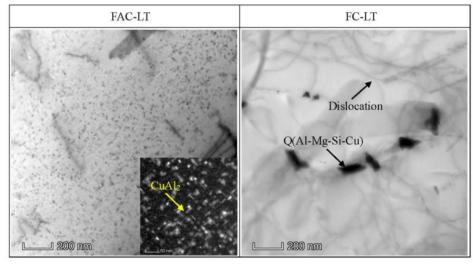

Fig. 7. STEM images for the FAC-LT , and FC-LT samples

4. Conclusions

This study examined the influence of the cooling rate on the extent of precipitation of cast ADC12. Based on the obtained experimental results, the following conclusions can be drawn:

1) A solid solution of Cu element occurred in the α-Al matrix during the casting process at cooling rates exceeding 0.03 °C/s (FAC). This cooling process could be replaced with a solid solution of T6 to induce the precipitation hardening of CuAl$_2$. The extent of the solid solution varied depending on the cooling rate; with a higher cooling rate, a more extensive solid solution was formed.

2) For the cast ADC12 sample cooled at a cooling rate > 0.03 °C/s, precipitation hardening occurred after the aging process. Furthermore, high Vickers hardness values were obtained for the GC and AC samples after aging at 175°C for 20 h. With higher temperature and longer heating process, over-aging occurred, resulting in lower mechanical properties.

Compliance with Ethical Standards:

Acknowledgements

References

[1] Sepehrband, P., Mahmudi, R. & Khomamizadeh, F. (2005). Effect of Zr addition on the aging behavior of A319 aluminum cast alloy. *Scripta Materialia*. 52(4), 253-257.

[2] Rana, G., Zhoua, J.E. & Wang, Q.G. (2008). Precipitates and tensile fracture mechanism in a sand cast A356 aluminum alloy. *Journal of Materials Processing Technology*. 207(1-3), 46-52.

[3] Tian, L., Guo, Y., Li, J., Xia, F., Liang, M. & Bai, Y. (2018). Effects of solidification cooling rate on the microstructure and mechanical properties of a Cast Al-Si-Cu-Mg-Ni piston alloy. *Materials*. 11(7), 1230.

[4] Choi, S.W., Kima, Y.M., Leea, K.M., Cho, H.S., Hong, S.K., Kim, Y.C., Kang, C.S. & Kumai, S. (2014). The effects of cooling rate and heat treatment on mechanical and thermal characteristics of Al–Si–Cu–Mg foundry alloys. *Journal of Alloys and Compounds*. 617, 654-659.

[5] Dobrzański, L.A., Maniara, R., Sokołowski, J. & Kasprzak, W. (2007). Effect of cooling rate on the solidification behavior of AC AlSi7Cu2 alloy. *Journal of Materials Processing Technology*. 191(1-3), 317-320.

[6] Shabel, B.S., Granger, D.A., Trucker, W.G. (1992). Friction and wear of aluminum-silicon alloys. In P.J. Blau (Eds.), *ASM Handbook: Friction, Lubrication, and Wear Technology* (pp. 785-794), ASM International.

[7] Son, S.K., Takeda, M., Mitome, M., Bando, Y. & Endo,T. (2005). Precipitation behavior of an Al–Cu alloy during isothermal aging at low temperatures. *Materials Letters*. 59(6), 629-632.

[8] Wen-jun, T., Lin, Q. & Pi-xiang, Q. (2007). Study on heat treatment blister of squeeze casting parts. *China Foundry*. 4(2), 108-111.

[9] Okayasu, M., Sahara, N. & Mayama, K. (2021). Effect of microstructural characteristics on mechanical properties of cast Al–Si–Cu alloy controlled by Na. *Materials Science and Engineering. A* (in press).

[10] Hamasaki, M. & Miyahara, H. (2013). Solidification microstructure and critical conditions of shrinkage porosity generation in die casting process of JIS-ADC12 (A383) alloy. *Materials Transactions*. 54(7), 1131-1139.

[11] Kamio, A. (1996). Refinement of solidification structure in aluminum alloys. *Japan Foundry Engineering Society*. 68, 1075-1083.

[12] Okayasu, M. & Go, S. (2015). Precise analysis of effects of aging on mechanical properties of cast ADC12 aluminum alloy. *Materials Science and Engineering. A* 638, 208-218.

[13] David, S.A. & Vitek, J.M. (1989). Correlation between solidification parameters and weld microstructures. *International Materials Reviews*. 34(1), 213-245.